International Journal of Heat and Mass Transfer 233 (2024) 126012

Contents lists available at ScienceDirect

International Journal of Heat and Mass Transfer

journal homepage: www.elsevier.com/locate/ijhmt

Thermal diffusivity characterization of semiconductive 1D micro/nanoscale structures

Amin Karamati [a,1], Meng Han [b,1], Xinyue Duan [c], Yangsu Xie [d,*], Xinwei Wang [a,*]

[a] Department of Mechanical Engineering, 271 Applied Science Complex II, Iowa State University, Ames, IA 50011, USA
[b] Shenzhen Institute of Advanced Electronic Materials, Shenzhen Institute of Advanced Technology, Chinese Academy of Sciences, Shenzhen, Guangdong 518055, PR China
[c] College of New Energy, China University of Petroleum (East China), Qingdao, Shandong 266580, PR China
[d] College of Chemistry and Environmental Engineering, Shenzhen University, Shenzhen, Guangdong 518055, PR China

ARTICLE INFO

Keywords:
Transient electrothermal (TET) technique
Nonlinear resistance-temperature relation
Semiconductive materials
Micro- and nanoscale
Graphene film
Single-walled carbon nanotubes

ABSTRACT

The transient electrothermal (TET) technique was developed and has been widely used for measuring the thermal diffusivity of fiber- and film-like materials at the micro/nanoscale. Upon step-current heating, the measured voltage-time (*V-t*) of the sample usually follows a sole increasing or decreasing trend, depending on the temperature coefficient of its electrical resistivity ($\theta_T = d\rho_e/dT$, ρ_e: electrical resistivity, T: temperature). Past physical mode for the *V-t* profile is based on an assumption that θ_T is constant during TET measurement, which applies to a large variety of materials. However, for semiconductive materials, θ_T depends on the charge carrier density and scattering time, and both vary with temperature. Therefore, θ_T has very strong nonlinear change with temperature, sometimes changes sign during TET measurement. This leads to abnormal *V-t* profiles that have never been addressed well, thereby making TET measurement not applicable for such scenarios. In this work, a new physical model is developed to consider the strong nonlinear relation between ρ_e and T to the third order. Our numerical modeling firmly proves the validity of this new model. Thin films of graphene (GreF) and single-walled carbon nanotube (SWCNTs) mat are measured using the TET technique over a wide temperature range: 84.5–690.9 K for the GreF, and 12–290 K for the SWCNT film. At a specific temperature for each sample, a semiconductive-to-metallic transition comes about and manifests in the resistance-temperature response, hence leading to abnormal TET signals. These TET signals are perfectly fitted using our nonlinear $\theta_T \sim T$ model to determine α. Intriguingly, the determined α of the GreF for the transition phase follows the overall $\alpha \sim T$ trend, confirming the robustness of the model. The obtained $\alpha \sim T$ trend is interpreted well using the thermal reffusivity theory and structure deterioration under temperature change. This work significantly extends the capability of TET to semiconductors for α measurement. Also, the new methodology developed for obtaining α at zero temperature rise significantly improves the measurement control and accuracy.

1. Introduction

One-dimensional (1D) micro/nanoscale materials hold significant importance across various fields due to their unique properties and versatile applications [1-4]. Thermal design, endurance, and stability of the systems depend critically on the thermophysical properties of 1D micro/nanostructures, particularly thermal conductivity (k) and thermal diffusivity (α). These thermophysical properties can be measured using a variety of either steady-state or transient techniques [5]. From among the transient ones, the transient electrothermal (TET) technique has proved to be a powerful and reliable one for both conductive and nonconductive micro/nanoscale wires or films. Fig. 1a shows the schematic of the TET technique. During the TET measurement, a step DC current is applied through the sample, which changes the resistance of the sample. This resistance change is reflected as voltage-time change, which is then used to fit to obtain the α of the sample. Not only does the TET technique offer fast and easy implementation [6], but it also provides well-defined heating over the tested sample. Moreover, the TET technique has been validated and used to characterize a wide variety of materials including polyester fibers and platinum wires [7], carbon and

* Corresponding authors.
E-mail addresses: ysxie@szu.edu.cn (Y. Xie), xwang3@iastate.edu (X. Wang).
[1] Equal contribution authors.

https://doi.org/10.1016/j.ijheatmasstransfer.2024.126012
Received 29 April 2024; Received in revised form 5 June 2024; Accepted 26 July 2024

graphene microfibers [8-11], carbon nanotubes [12-14], graphene paper [15], SiC microwires [16], carbon nanocoils [17], gas diffusion layers of fuel cells [18], polypropylene separator of lithium-ion batteries [19], etc. The dimensions of these samples along with their measured α values, are summarized in Table 1. Details of the TET technique will be discussed in Section 2.

For most materials, the TET signal (voltage vs. time) is in the form of either pure monotonic increasing or decreasing, depending on their temperature coefficient of resistivity ($\theta_T = d\rho_e/dT$, ρ_e: electrical resistivity, T: temperature). For a small temperature rise during TET measurement, θ_T can be treated as constant. However, it turns out that for some materials, such as semiconductors, this transient response deviates significantly from that pure form of evolution and turns into abnormal forms. Fig. 1b shows the typical normal TET signals, whether pure increasing ($\theta_T > 0$) or pure decreasing ($\theta_T < 0$) along with an abnormal one. It should be noted that the form of abnormality can vary for different materials and conditions. The physical reason of this abnormality is that θ_T is not a constant during TET measurement, rather it changes significantly, or even changes sign.

For graphene paper, Xie et al. [20] reported a transition from a pure increasing TET profile to a pure decreasing one within the 290–70 K temperature range. They reported a combined trend in single TET signals for the 245–210 K temperature range. The fitting of normal TET signals (whether pure increasing or decreasing) was done using a function in the form of $T^* = 1 - 0.99\exp(-9.911 \times \alpha t/L^2)$, while the abnormal ones were fitted using a new mathematical model in the form of $T^* = a[\exp(-9.911 \times \alpha_1 t/L^2)] + b[\exp(-9.911 \times \alpha_2 t/L^2)] + c$. Here T^* is the normalized temperature rise, α is thermal diffusivity, t is time, and L is the sample length. Although this two-exponential function model was used for their data processing of abnormal TET signals, the results seemed to be somehow arbitrary, and a physical connection between α_1 and α_2 lacks. These abnormal TET signals have not been explained in the past, and they have emerged more due to some special physics behind them.

As stated earlier, for normal TET signals that the resistance (R) change of the sample brings about that transient voltage behavior, it is considered that the change in R linearly correlates with T change during step heating, and the corresponding signals are processed accordingly. The abnormal TET signals might imply other physics relationships between R change and T in the sample, and no physics has been established so far to fit abnormal TET signals to determine α. The R-T relation could be nonlinear for semiconductive materials, changing from positive to negative for the θ_T (or vice versa). The transition in θ_T sign can be explained by the fact that θ_T ($d\rho_e/dT$) is a function of both dn/dT and $d\tau/dT$ [9] as $\rho_e = m/(ne^2\tau)$, where m is the electron mass, n the number density of conduction electrons, and τ the characteristic electron scattering time. An increase in sample temperature will excite more electrons to the conduction band, thereby increasing n. [9] τ is determined by scattering by defects and impurities and scattering by "phonons", or lattice vibrations. While the scattering rate by defects and impurities have negligible effect of temperatures, the temperature increase will increase the population of phonons that are involved in electron scattering. Therefore, it is expected $d\tau/dT$ is negative. The combined effects of these terms (i.e., dn/dT and $d\tau/dT$) in a T range in semiconductive materials not only lead to a sign transition in θ_T, but also lead to abnormal TET signals at some temperatures when θ_T changes its sign during TET measurement.

Table 1
Characteristics of some micro/nanoscale samples studied via TET.

Sample	Diameter/ thickness (μm)	Length (μm)	α_{eff}@ ~ 290 K ($mm^2\ s^{-1}$)
Polyester fiber [7]	~10.0	~590–680	~ 0.52–0.66
Platinum wire [7]	25.4	~5000	25.3–27.8
Graphene fiber [8]	28.2	1959	0.74
Carbon fiber [9]	55.2	~2000	1.32
Carbon nanotube (CNT) bundles [14]	222–280	2370–2770	13.2–29.6
Graphene paper [15]	12.3	1660	0.99
SiC microwires [16]	34.29	1495	2.89
The gas diffusion layer of fuel cells [18]	100	3752	5.3
Polypropylene separator [19]	25	2900	0.66

In this work, we devise a theory to consider the nonlinear R-T relation in 1D semiconductive materials for the measured V-t curve for data processing. This theory is rigorously validated by numerical modeling and characterization and is then used to determine the α of thin films made of graphene (GreF) and single-walled carbon nanotube (SWCNT) over a very large T range. The development of this physical model significantly extends the capability of the TET technique to measure α of semiconductive materials from the microscale down to the nanoscale.

2. Nonlinear R-T response: theoretical development

2.1. Physics development

The TET technique, developed by our lab in 2007 [7], has proven to be highly effective in accurately measuring the in-plane α of materials in the form of fibers or films. In this method, the sample is suspended over a trench and secured with silver paste to the electrodes, establishing robust electrical and thermal connections between the sample and electrodes (Fig. 1a). The measurement process involves inducing a transient voltage rise over the sample through Joule heating using a step DC current (I_0). The resulting transient T variation, represented by the

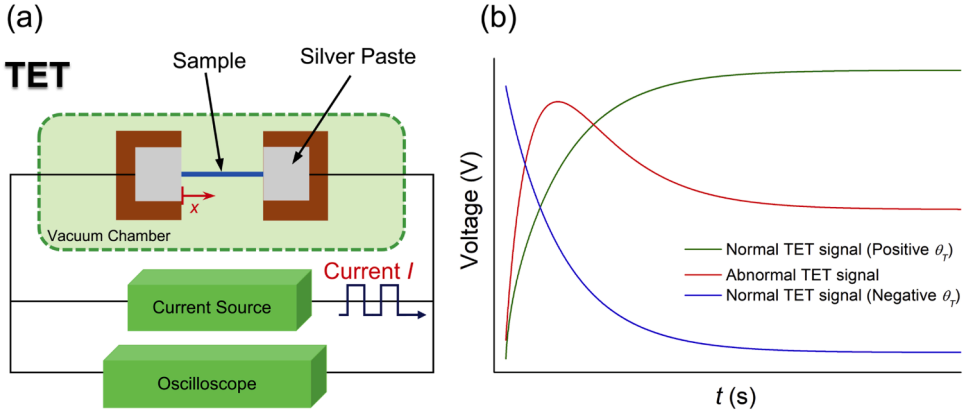

Fig. 1. (a) The schematic of the TET technique. (b) Demonstration of normal (pure increasing or decreasing) and abnormal TET signals (V-t). Abnormal signals can be of different varieties in shape.

voltage rise or drop over the sample, is then utilized to determine α. Given the high length-to-thickness ratio of the sample, it is reasonable to assume one-dimensional heat conduction along the sample. The transient heat conduction along the sample's length (i.e., along the x-axis) is governed by the below equation [7]:

$$\frac{\partial(T\rho c_p)}{\partial t} = \frac{\partial}{\partial x}\left(k\frac{\partial T}{\partial x}\right) + \dot{q}, \tag{1}$$

where ρ, c_p, and k are the density, specific heat, and thermal conductivity of the sample, respectively. t is time, and $\dot{q}$ in Wm^{-3} denotes the equivalent volumetric heating generated by the electrical current. Solving Eq. (1) using the integral of Green's function results in the T variation along the sample's length, which can be represented as [7]:

$$T(x,t) = T_0 + \frac{\alpha}{k}\int_{\tau=0}^{t}\int_{x'=0}^{L} q_0 G_{X11}\, dx' d\tau, \tag{2}$$

where G_{X11} is the Green's function given as:

$$G_{X11}(x,t|x',\tau) = \frac{2}{L}\sum_{m=1}^{\infty}\exp\Big[- m^2\pi^2\alpha(t-\tau)/L^2\Big] \times \sin\left(m\pi\frac{x}{L}\right)\sin\left(m\pi\frac{x'}{L}\right). \tag{3}$$

The normalized transient average temperature rise over a sample of length L is [7]:

$$T^* = \frac{96}{\pi^4}\sum_{m=1}^{\infty}\frac{1-\exp\Big[-(2m-1)^2\pi^2\alpha t/L^2\Big]}{(2m-1)^4}. \tag{4}$$

In Eq. (4), t can be normalized using the Fourier number as $Fo = \alpha t/L^2$. Upon step heating during the TET measurement, the sample's temperature rise will bring about changes in its resistance, then leading to a transient voltage change across the sample, which finally reaches a steady state. For normal TET signals (R has a linear relation with T), taking $\Delta\rho_e = \theta_T\Delta T$, it can be deduced that the electrical resistance change (ΔR) of the sample is linearly related to the average temperature rise ($\overline{\Delta T}$) of the sample as: $\Delta R = \theta_T\beta\overline{\Delta T}$, where $\beta = L/A$ with A as the cross-sectional area of the sample. A simplified form of the average temperature rise of the sample has been developed in our recent work [12]:

$$\overline{\Delta T} = a_1 + a_2\exp\big(-\pi^2 Fo\big). \tag{5}$$

where a_1 and a_2 are just coefficients. For normal TET signals, due to the linear correlation between resistance and temperature, ΔR and ΔV also follow the same expression as Eq. (5). To demonstrate this, considering a sample with an arbitrary length of 0.7 mm, the temperature evolution of 25 locations (equally distanced) of the sample is calculated using Eq. (2). For this calculation, q_0, α, and k take 1×10^9 Wm^{-3}, 2×10^{-5} $m^2\,s^{-1}$, and 40 $Wm^{-1}\,K^{-1}$, respectively. The results of temperature rise vs. Fo for selected locations (based on the existing symmetry) are shown in Fig. 2a. Note that $\xi = x/L$, where x is the location on the sample, and its starting point is the contact point with the electrode.

The average temperature rise of the sample is calculated based on the temperature rises of different locations and is shown to the left axis of Fig. 3a. This figure also shows the fitting of the average temperature rise of the sample using Eq. (5). As can be seen, this fitting looks very good with fitted values of 0.999 and −0.988 for a_1 and a_2. Note that the fitted value of a_1 is almost equal to the steady state value of $\overline{\Delta T}$, and that of a_2 is nearly the negative of the steady state value for $\overline{\Delta T}$.

For abnormal TET signals, here we detail the work to relate the measured ΔV and the temperature rise. Since ΔR nonlinearly correlates with the temperature rise of the sample, for sound accuracy, the electrical resistivity can be assumed to correlate with the temperature change as: $\Delta\rho_e = a\Delta T + b(\Delta T)^2$. Integrating this equation over the whole sample's length, the total electrical resistance change can be obtained as $\Delta R = \beta\left[a\overline{\Delta T} + b\overline{(\Delta T)^2}\right]$. Using the calculated temperature rise of different locations on the sample, the average squared temperature rise of the sample is computed and shown in Fig. 3a. Note that the temperature rise of each location is first squared, and then the average value is obtained. To fit this profile, we design a function as

$$\overline{(\Delta T)^2} = b_1 + b_2\exp\big(-\pi^2 Fo\big) + b_3\exp\big(-2\pi^2 Fo\big). \tag{6}$$

The design of Eq. (6) is based on Eq. (5), for which we proved that the coefficient of Fo is $-\pi^2$ [8]. This conclusion can be extended to the temperature rise of any local point of the sample. To elaborate more on this point, we calculate $\ln(\Delta T_1 - \Delta T)$ in a Fo range for different locations of the sample studied above, whose local temperature rises are already shown in Fig. 2a. Here ΔT_1 is the steady state temperature rise. Fig. 2b shows that all the $\ln(\Delta T_1 - \Delta T)$ for different locations tend to become linear after a very small initial nonlinearity. Very interestingly, the slope of all linear profiles vs. Fo is $-\pi^2$. So, by simply squaring the local temperature rise, it can be concluded that $\overline{(\Delta T)^2}$ will have the terms of $\exp(-\pi^2 Fo)$ and $\exp(-2\pi^2 Fo)$, thereby leading to the expression of Eq. (6). The result of the fitting for theoretically calculated $\overline{(\Delta T)^2}$ using Eq. (6) is shown in Fig. 3a. As can be seen, the fitting looks excellent, and the fitted values for $\overline{(\Delta T)^2}$ parameters are 1.25, −2.49, and 1.24 for b_1, b_2, and b_3, respectively. Consequently, since we assume that $\Delta\rho_e = a\Delta T + b(\Delta T)^2$, the final $\overline{\Delta R}$ is related to Fo as:

$$\overline{\Delta R} = d_1 + d_2\exp\big(-\pi^2 Fo\big) + d_3\exp\big(-2\pi^2 Fo\big) \tag{7}$$

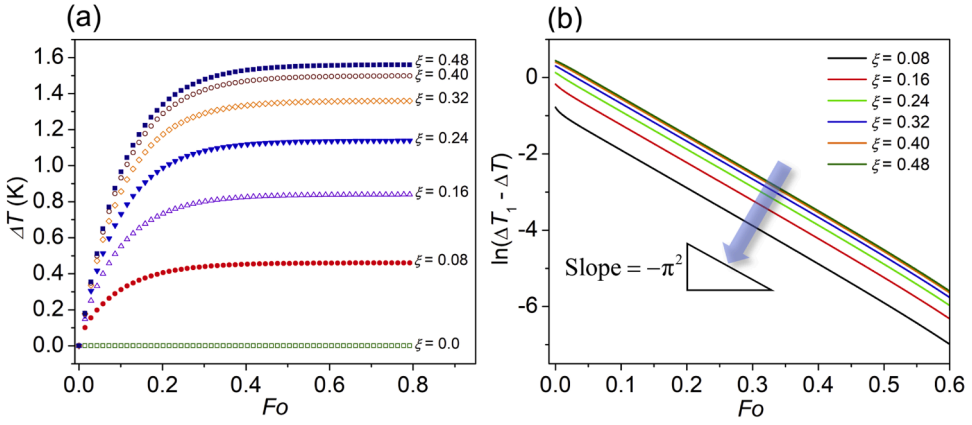

Fig. 2. (a) Temperature evolution of different locations ($\xi = x/L$) of the sample calculated using the solution of the TET [Eq. (2)]. (b) Natural of steady-state temperature rise subtracted by the temperature rise with Fo for different selected locations, the slope of which is used to support the model development.

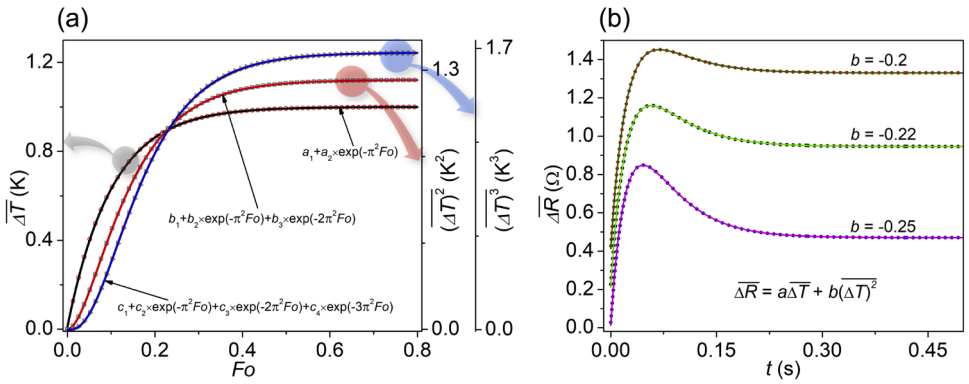

Fig. 3. (a) The average (left axis), average squared (1st right axis), and average cubed (2nd right axis) temperature rise of the sample calculated based on the temperature rises of different locations. The figure also includes their fitting curves (solid lines) using the corresponding functions. (b) Generated average resistance variation with time (dots) for a given 1D sample using numerical modeling, considering different b values based on the relation $\Delta\rho_e = a\Delta T + b(\Delta T)^2$ in the model. The fitting results of these R-t responses using Eq. (7) are illustrated as solid lines. Note that an offset of +0.4 and +0.2 Ω is applied to the $b = -0.2$ and −0.22 graphs for better representation.

The voltage change of the sample with time can be described using the same function as Eq. (7). Such formula can be used to fit the measured V~t data to determine α. For a stronger nonlinear relation between $\Delta\rho_e$ and ΔT, a third-order polynomial relation can be used as $\Delta\rho_e = a\Delta T + b(\Delta T)^2 + c(\Delta T)^3$. For $\overline{(\Delta T)^3}$, it can be expressed as

$$\overline{(\Delta T)^3} = c_1 + c_2\exp(-\pi^2 Fo) + c_3\exp(-2\pi^2 Fo) + c_4\exp(-3\pi^2 Fo). \quad (8)$$

The theoretical calculation and the fitting results are shown in Fig. 3a. The fitted parameters are calculated to be $c_1 = 1.67$, $c_2 = -5.05$, $c_3 = 5.08$, and $c_4 = -1.71$. As a result, the resistance change can be expressed as

$$\overline{\Delta R} = g_1 + g_2\exp(-\pi^2 Fo) + g_3\exp(-2\pi^2 Fo) + g_4\exp(-3\pi^2 Fo). \quad (9)$$

These functions are achieved using the combination of the functions introduced for $\overline{\Delta T}$, $\overline{(\Delta T)^2}$, and $\overline{(\Delta T)^3}$. The coefficients "g" are related to the resistance change with temperature and could vary sample to sample. Finally, the measured V~t result can be fitted using an expression in the form of:

$$V = f_1 + f_2\exp(-\pi^2 Fo) + f_3\exp(-2\pi^2 Fo) + f_4\exp(-3\pi^2 Fo) \quad (10)$$

to determine α. Eq. (10) is based on Eq. (9) considering the fact that: $V = I_0\cdot\overline{\Delta R} + V_0$. V_0 is the voltage at the beginning of the step current. So, the relationship between the coefficients in Eqs. (10) and (9) are $f_1 = V_0 + I_0\cdot g_1$, and $f_i = I_0\cdot g_i$ ($i = 2, 3, 4$). These coefficients (i.e., f_1, f_2, etc.) can be obtained from fitting the experimental data (TET signal).

2.2. Validation of the theory based on numerical TET experiment

In this section, we will prove the validity of the theory developed above. Here, we first use a numerical program to calculate the R-t response of a sample under a nonlinear R-T relation upon step DC current heating. In this TET numerical experiment, the heat conduction within the sample subjected to step Joule heating is solved. This modeling has the ability of a comprehensive consideration of spatial property (i.e., k, ρc_p, and θ_T) distribution along the sample's length. But here, we consider the properties to be constant along the sample's length, except θ_T. The modeling is based on the finite volume method utilizing an implicit algorithm. The time step is set at 0.2 ms, and the mesh size is 1 μm. The TriDiagonal Matrix Algorithm (TDMA) is applied to solve the equations. It should be mentioned that the calculated resistance change (response) in the model takes into account the rise in temperature at each point. The model sample's L, k, and ρc_p are 1 mm, 3 Wm^{-1} K^{-1}, and 1.5 × 10^6 Jm^{-3} K^{-1}, respectively. The sample's diameter is considered to be 28 μm and the unit heating power is calculated to be 1.0 × 10^8 Wm^{-3}. Moreover, as the R-T relationship is considered to be nonlinear [$\Delta\rho_e = a\Delta T + b(\Delta T)^2$], the value of a is 1, and three different values of −0.2, −0.22, and −0.25 are chosen for b. These values are deliberately chosen to generate different abnormal responses commonly observed in experiments, which will be discussed in the next sections. Additionally, the choice of 2nd order nonlinearity is based on its higher likelihood of existence in real-world scenarios over a small temperature range. The generated R-t responses for different b values are shown as dots in Fig. 3b. It should be noted that corresponding graphs for the $b = -0.2$ and −0.22 are offset by +0.4 and +0.2 Ω for the sake of visualization. These profiles are then fitted using Eq. (7), in which Fo has been replaced with $\alpha t/L^2$ [i.e., $\overline{\Delta R} = d_1 + d_2\exp(-\pi^2\alpha t/L^2) + d_3\exp(-2\pi^2\alpha t/L^2)$] to obtain d_1, d_2, and d_3, and α. The fitting results are shown as solid lines in Fig. 3b. Sound fitting has been achieved, and the fitted values for the parameters are given in Table 2.

In our modeling, α of the sample is 2 mm^2 s^{-1} [$k/\rho c_p = 3/(1.5\times10^6)$]. Interestingly, the fitted values for α using the defined function are either the same or very close to the value used in the modeling, with only 0.5 % error. This firmly confirms the validity of the developed physical model for abnormal TET signals. In following next sections, we will process experimental data fitting using the two- and three-exponential functions to not only achieve the best fitting but also unravel the order of the R-T relationship.

3. Thermal diffusivity measurement of semiconductive graphene film

In this section, we discuss the TET experiments done on the graphene film (GreF) provided by our partner. The GreF is typically manufactured through a process involving layer-by-layer stacking of graphene oxide sheets, followed by subsequent reduction and graphitization [21]. To conduct TET measurements, the film is precision-cut into narrow strips, becoming 210 μm wide, 14.55 mm long, and 30 μm thick. The strip is then suspended between two aluminum electrodes, which also act as heat sinks for the sample. Copper pieces, serving as clamps and secured with screws, are employed to enhance the contact between the sample

Table 2
Fitted parameters for the simulated R-t response.

#	Case	d_1	d_2	d_3	α (mm^{2}s^{-1})
1	$b = -0.2$	0.930	0.955	−1.869	2.01
2	$b = -0.22$	0.746	1.327	−2.057	2.01
3	$b = -0.25$	0.470	1.882	−2.336	2.00

and the electrodes, minimizing both electrical and thermal contact resistance. The method of using copper pieces as clamps instead of silver paste has also proved very reliable for securing good electrical and thermal contacts between the sample and the electrodes, especially for thick and porous samples. Our group has had such experience in the past in sample preparation [22]. Subsequently, the sample base is affixed to the heating/cooling head within a vacuum chamber. The TET measurements are done in a temperature range between 84.5 and 690.9 K, and the voltage change history of the sample is recorded. All the TET tests are done under vacuum condition (~10^{-3} Pa). Fig. 4a and b show the top and side view SEM images of the GreF sample, respectively, to show how the sample looks like under higher resolutions. This could help understand the physical structure behind its moderate thermal diffusivity. As can be seen, surface wrinkles formed during the compression process following graphitization [21]. It is important to note that based on Fig. 4b, taken from the cross-section of the GreF, wrinkles can be found in the deep structure in addition to the sample surfaces. Additionally, Fig. 4b illustrates the relatively loose and porous stacking of layers of the GreF structure.

Starting from 84.5 K, the TET voltage signal shows a sole decreasing trend. These signals can be fitted using the single exponential function [i.e., only the first exponential term in Eq. (10)], and the fitted α values are given in Fig. 5d as blue symbols. A decreasing trend is observed for the α with increased T, changing from 1.57×10^{-3} m^2 s^{-1} at 84.5 K to around 2.70×10^{-4} m^2 s^{-1} at 503 K. When T reaches ~530 K, the TET signal starts to exhibit an abnormal profile until ~630 K. Within this temperature range (i.e., 530–630 K), a semiconductive-to-metallic transition comes up as the TET voltage signals turn from a pure decreasing form at < 530 K to a pure increasing trend after ~630 K. This transition indicates a switch in θ_T sign from negative to positive. This can be explained using Fig. 5e, in which the resistance variation with temperature is given. The resistance at each temperature is calculated using the applied current and the final induced voltage in the sample. The resistance has a downward relation with temperature (semiconducting behavior) and then an upward one (metallic behavior). Magnifying the transition region (the inset in Fig. 5e) shows that a clear transition comes

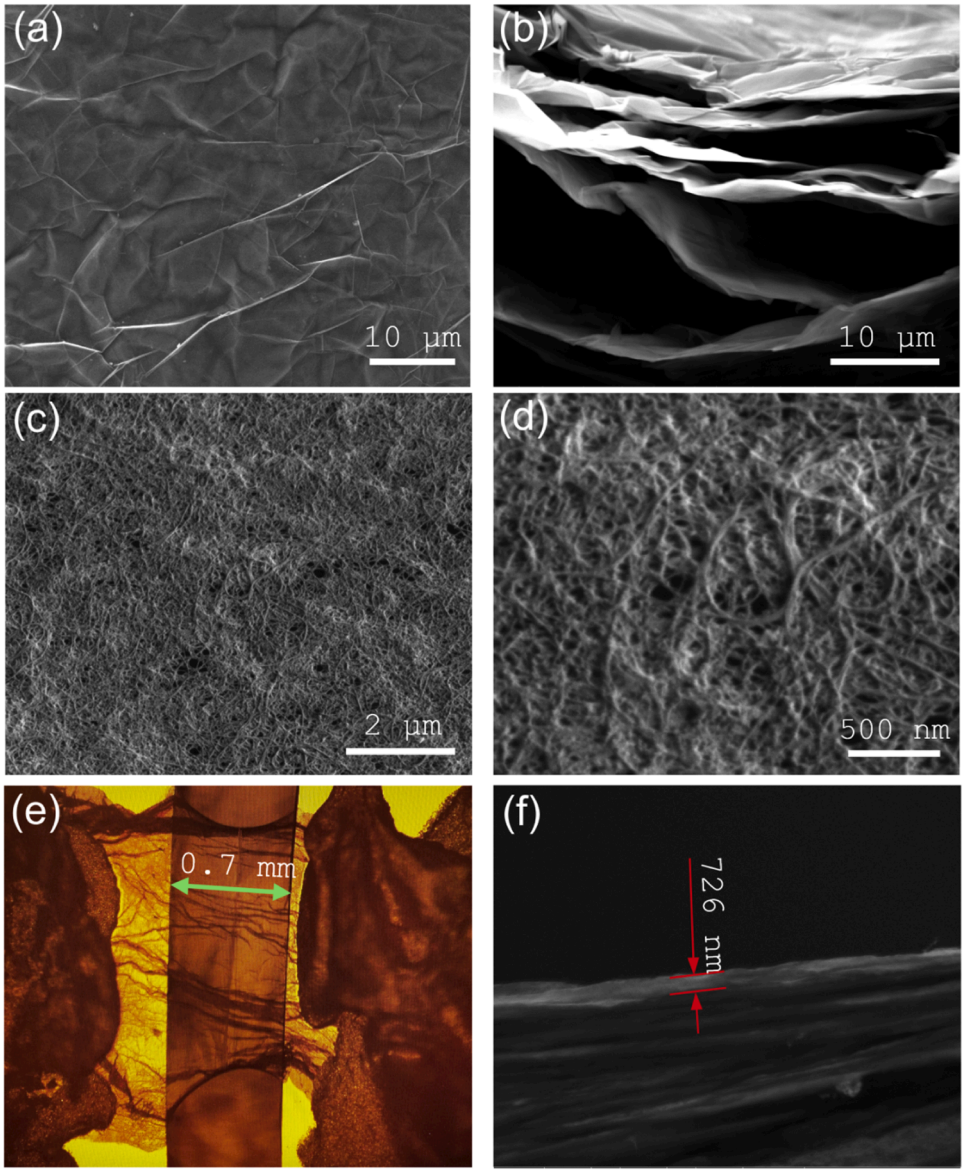

Fig. 4. The GreF sample's SEM images from the (a) top and (b) side views under 2000 × and 5000 × magnifications, respectively, revealing wrinkles on the sample's surface and its porous structure, respectively. The SEM images of the SWCNT film under (c) 15000 × and (d) 50000 × magnifications show the sample's curly morphology. (e) The optical image of the SWCNT thin film showing the length of the suspended part. (f) The side view SEM image of the SWCNT film under 5000 × is used to measure the sample's thickness.

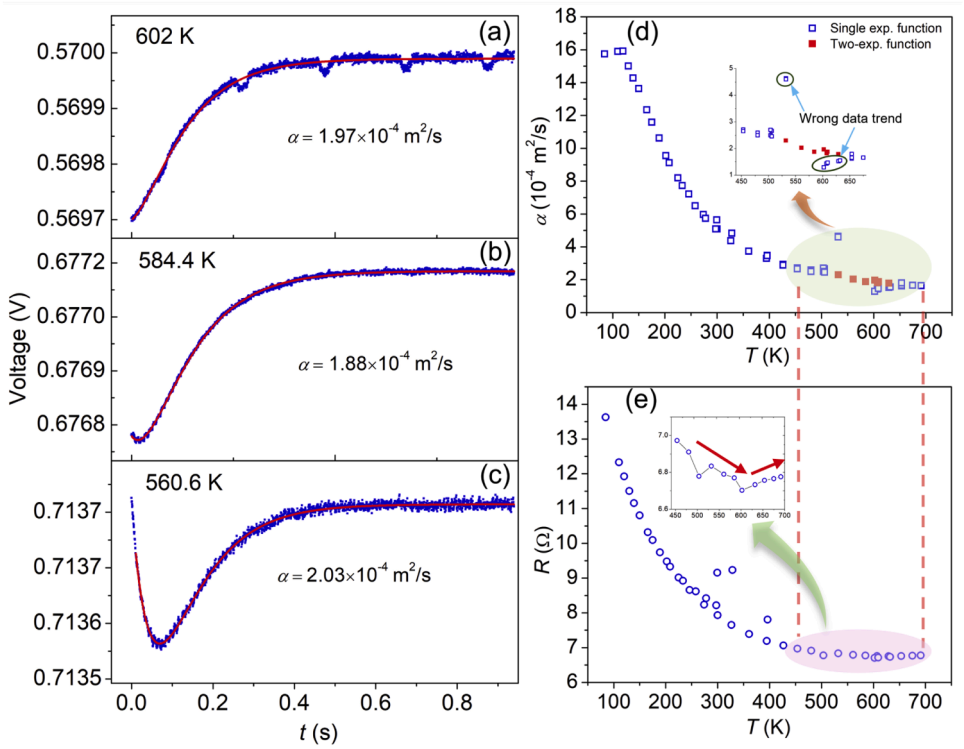

Fig. 5. TET signals of the GreF sample in the transition range along with their fittings using two-exponential function at (a) $T = 602$, (b) 584.4, and (c) 560.6 K. (d) Thermal diffusivity variation of the GreF sample with temperature calculated using either single or two-exponential functions. The inset emphasizes the inappropriateness of using the single exponential function for the transition range. (e) Resistance vs. temperature change for the GreF. The inset emphasizes the θ_T sign change within the transition region from semiconducting to metallic behavior.

about, leading to the transition in signal from decreasing to increasing. The mechanism and physics behind this transition were explained from the viewpoint of carrier transport and scattering mechanism in the Introduction, elaborating on the competition between carrier mobility and carrier density, which is the key to θ_T determination.

Fig. 5a–c show some TET signals ($T = 602$, 584.4, and 560.6 K) taken from the GreF sample in the transition range. For $T = 560.6$ K (Fig. 5c), for instance, the signal experiences a downward part following a rising part until reaching the steady state. This trend is quite like the signal at $T = 584.4$ K (Fig. 5b) with a more initial descending part. This initial decreasing part has almost faded at $T = 602$ K (Fig. 5a). The main point about this transition range is that due to the complexity of their TET signals, the thermal diffusivity could not be obtained using the single exponential function [21]. Using the single exponential function, neither the quality of the fittings is good, nor the obtained α values follow the main trend. This deviation from the main trend is emphasized using the inset in Fig. 5d for $T = 532$–631.8 K. This clearly shows that the TET signals of these temperatures cannot be fitted using the single exponential function. So, the two-exponential function [i.e., the first two exponential terms in Eq. (10)] is used here to fit these abnormal signals. Based on Fig. 5a–c, the fittings look excellent for the signals of $T = 602$, 584.4, and 560.6 K. Moreover intriguingly, the α values (red squares in Fig. 5d) obtained using the two-exponential function make the overall trend continuous and smooth. This firmly proves the validity of the two-exponential function model. The corresponding values of the fitted parameters (b_1, b_2, b_3, and α) are obtained to be 0.71374, −0.00069, 0.00069, and 2.02×10^{-4} m^2 s^{-1}, for $T = 560.6$ K, and 0.57003, −0.00051, 0.00022 and 1.97×10^{-4} m^2 s^{-1} for 602 K signals. The TET fitting uncertainty for thermal diffusivity determination have been systematically studied by our group in the past [8], and it is ~0.2 % or less. Also, the length measurement has an uncertainty less than 2 %. Therefore the final α has an uncertainty less than 5 %.

Based on Fig. 5d, the α of the GreF experiences a decreasing trend with temperature, dropping from 15.9×10^{-4} m^2 s^{-1} at $T = 110$ K to 1.64×10^{-4} m^2 s^{-1} at 691 K. This decrease can be interpreted using heat carrier transport theory. It is common knowledge that phonon propagations drive thermal transport in carbon-based materials, including GreF, with insignificant electron contributions. Different phonon scattering mechanisms, namely Umklapp phonon-phonon (U-scattering), boundary scattering (b-scattering), defect scattering (d-scattering), and interface-induced scattering (i-scattering) affect the heat transport capability of the GreF. Our lab initially introduced the thermal reffusivity ($\Theta = 1/\alpha$ for phonons) model to directly quantify the phonon scattering intensities in materials, such as graphene foams, CNT coils, ultrahigh molecular weight polyethylene, and $MoSe_2$, etc. [23-26]. Based on a single relaxation time approximation [27,28], the thermal reffusivity can be expressed as: $\Theta = 3v^{-2}\left(\tau_U{}^{-1} + \tau_i{}^{-1} + \tau_d{}^{-1} + \tau_b{}^{-1}\right)$, where τ is the relaxation time of phonon scattering. As the temperature drops, there is an increase in τ_U because both the lattice vibration and U-scattering become weaker. U-scattering will diminish when the temperature drops further and reaches around 0 K, leaving behind i-, b- and d-scattering, which are primarily affected by grain size and defect level and barely alter with temperature. Also, for materials with solid structure (i.e., the structure is stable with temperature change), the i-scattering effect is insignificant. Consequently, Θ will increase with increased temperature, meaning α decreases with increased temperature, as seen in Fig. 5d.

4. Thermal diffusivity measurement down to 12 K with 0 K temperature rise: SWCNT film

In this section, the TET experiments conducted on a SWCNT film will be discussed. The film is composed of randomly connected SWCNTs and is suspended using two Al-coated pieces of Si/SiO_2 as electrodes attached to a glass slide. The length and thickness of the film are measured to be 0.7 mm and 726 nm (Fig. 4e, f). The width of the sample

is narrowed to around 19 μm by cutting it using a laser after the sample is suspended. Silver paste is used to secure the contact points between the electrodes and the film to ensure reliable electrical and thermal contacts. Usually, the electrical contact resistance using silver paste is less than 1 Ω. As the electrical resistance of the SWCNT film sample is more than 1 kΩ, using silver paste to secure the connection is safe and acceptable. The TET tests are done in a temperature range from 290 K to 12 K in vacuum condition (<1 mtorr) inside a cryogenic system (CCS-450, JANIS). The glass slide is used to electrically separate the sample from the rest of the cryogenic system. The SEM images of the sample indicated the curly morphology of the SWCNT film in 15,000 × and 50,000 × shown in Fig. 4c and d. These figures will be used to explain why the α values of the SWCNT film are much smaller than those of aligned SWCNT bundles studied in our past work [29]. Based on these figures, a dense curly morphology is observed for the SWCNT film. It should be noted that at each temperature, the TET test is done using different step current values. The reason for doing this will be explained later.

The TET signals at the ambient (chamber) temperature of 290 K with different I_0 values of 0.3, 0.4, and 0.52 mA are shown in Fig. 6a. As can be seen, the voltage change shows an increasing trend with time, indicating a positive (metal-like) θ_T for the sample. The TET signals are then fitted using Eq. (5) to obtain their α. Based on Fig. 6a, the fittings are perfectly accomplished, with the corresponding α values of 1.72×10^{-5}, 1.52×10^{-5}, and 1.32×10^{-5} m^2 s^{-1} for I_0 of 0.3, 0.4, 0.52 mA. The corresponding fitted values for parameters a_1 and a_2 are obtained to be 0.3348 and −0.0011 for $I_0 = 0.4$ mA, for instance. For $T = 210$ K, the signals show an abnormal form shown in Fig. 6b. The TET voltage signal at this temperature first goes up and then descends and reaches a steady state. The physical explanation behind such transition was explained in the Introduction. However, it can also be explained using the *R-T* evolution in the vicinity of $T = 210$ K (shadowed part) in Fig. 7a. As it has

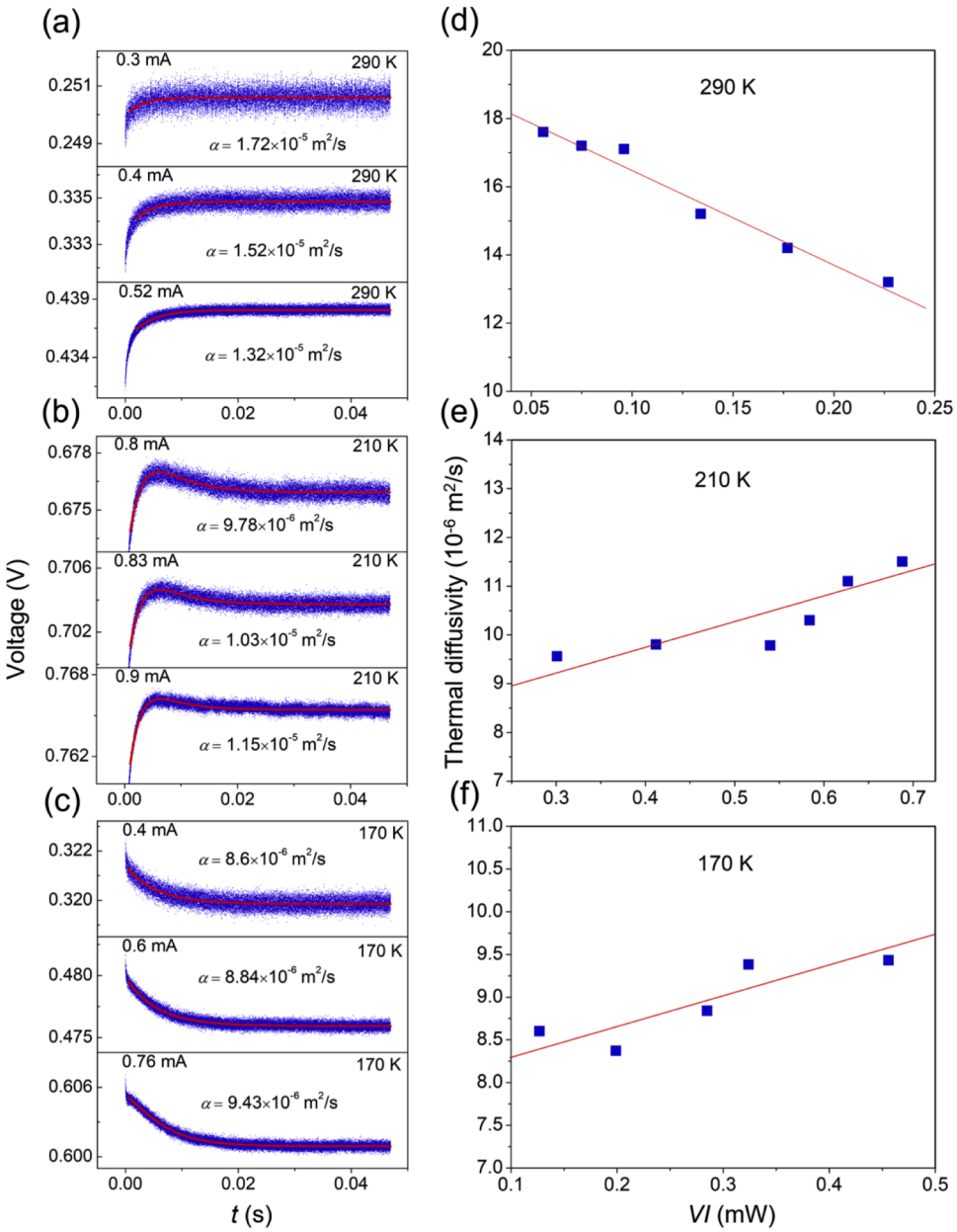

Fig. 6. The TET signals of the SWCNT film with different current values at ambient temperatures of (a) $T = 290$ K, (b) 210 K, and (c) 170 K. The single exponential function is used for the $T = 290$ K signals fitting, while the two-exponential function is utilized for the $T = 210$ K and 170 K ones. (d)(e)(f) show the thermal diffusivity variation of the SWCNT film vs. heating level at ambient temperatures of $T = 290$ K, 210 K, and 170 K.

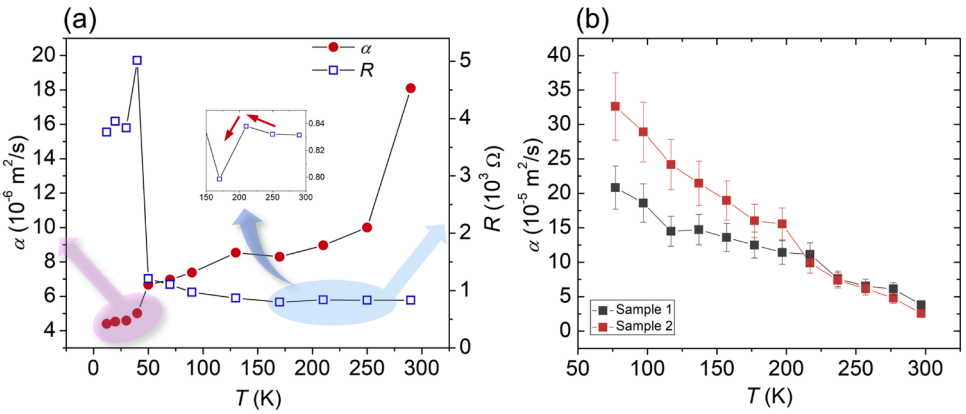

Fig. 7. (a) Thermal diffusivity (left axis) and resistance (right axis) evolution of the SWCNT film with temperature. The inset shows the change in the θ_T sign at ~210 K. (b) Thermal diffusivity variation of two highly aligned SWCNT bundles with temperature. Reproduced with permission from Ref. [29]. Copyright 2023. Elsevier.

been magnified in the inset in Fig. 7a, a clear transition in θ_T sign is seen at around $T = 210$ K. These signals cannot be fitted using the single exponential [i.e., only the first exponential term in Eq. (10)] function. So, they are fitted via both two-exponential [i.e., the two first exponential terms in Eq. (10)] and three-exponential [i.e., Eq. (10)] functions. A nice fitting is achieved using both functions for the signals at $T =$ 210 K, but a lower fitting mean square error (MSE) is achieved using the two-exponential function. This makes sense as the existence of dependency between the $\overline{\Delta R}$ and $\overline{(\Delta T)^3}$ is quite rare. For $I_0 = 0.83$ mA, for instance, the corresponding MSE of the fitting for the two- and three-exponential functions are calculated to be 1.23×10^{-8} and 7.44×10^{-8}. Consequently, we proceed with the two-exponential function for the rest of the abnormal TET signals. Other fitting parameters, b_1, b_2, and b_3, are obtained to be 0.7036, 0.006, and −0.01, respectively, for $I_0 =$ 0.83 mA. As shown in Fig. 6b, α values of 9.78×10^{-6}, 1.03×10^{-5}, and 1.15×10^{-5} m^2 s^{-1} are obtained for $I_0 = 0.8$, 0.83, and 0.9 mA, respectively, at $T = 210$ K. At $T = 170$ K, the signals are still not in the pure decreasing form that can be fitted using the single exponential function. This can be especially observed in the signals with higher I_0 values in Fig. 6c. So, here, we again use the two-exponential function for the signal fitting. For $I_0 = 0.6$ mA, for example, b_1, b_2, and b_3 are obtained to be 0.6009, 0.0072, −0.0028, and the α is 9.43×10^{-6} m^2 s^{-1}.

The reason for conducting the TET test with different I_0 values at each temperature point is due to a specific issue with the TET technique that it does not account for temperature rise when determining α. In fact, the measurement of α during the TET is not performed at the intended ambient temperature because of the temperature rise occurring when I_0 is applied. In the TET experiment, the sample's temperature rises by at least 1 K for each 0.3 % increase in voltage [24]. Electrical resistance changes with temperature relatively slowly at low ambient temperatures of 50 K or less. Hence, a higher temperature increase is associated with a 0.3 % voltage/resistance change for lower ambient temperatures. In order to guarantee acceptable sensitivity and reliability for TET measurement, a minimum relative voltage change of ~0.3 % is typically needed. Here, the TET measurements are carried out using various currents to make a range of voltage/resistance change from ~0.3 % to ~1 % for each ambient temperature point to find the sample's α at an ambient temperature with zero temperature rise. This is done by plotting the α value against the heating power for each measurement case. Intriguingly, this plot follows a good linear trend, the intercept of which is the α at the ambient temperature point with zero temperature rise during the test. Based on Fig. 6d–f, the α values with zero temperature rise for ambient temperatures of 290 K, 210 K, and 170 K are calculated to be 1.81×10^{-5} m^2 s^{-1}, 8.96×10^{-6} m^2 s^{-1}, and 8.3×10^{-6} m^2 s^{-1}, respectively.

To the left axis of Fig. 7a, the SWCNT film's thermal diffusivity variation with temperature is plotted out. As can be seen, starting from 290 K downward, α of the sample starts to decrease quite monotonously from 1.81×10^{-5} m^2 s^{-1} to 5.02×10^{-6} m^2 s^{-1} at $T = 40$ K. Then, the α value levels off to around 4.0×10^{-6} m^2 s^{-1} at $T = 12$ K. Here the trend of α-T is opposite to what we earlier showed for the GreF sample. Rahbar et al. [29] also reported a decreasing trend for α with increased temperature for highly aligned SWCNT bundles (Fig. 7b), elaborating on it using the thermal reffusivity theory, as discussed for the GreF in Section 3.

For the GreF and short and highly aligned SWCNTs, the defect level is low. Also, the structure is stable under temperature change. As a result, the contribution from interface-induced and defects-induced phonon scattering are not strong, making the U-scattering dominant in Θ-T behavior. As temperature decreases, Θ gets smaller due to the U-scattering vanishment (τ_U becomes bigger). So, α as the inverse of Θ increases with temperature reduction. For the SWNCT film measured in this work, however, the structure is composed of random, loosely connected nanotubes (Fig. 4c, d). π-π interactions and van der Waals forces indeed play a significant role in the interactions between nanotubes in the SWCNT film. These interactions are relatively weak compared with other types of chemical bonds and provide strong phonon scattering. So, the i-scattering becomes dominant in this case, surpassing the U-scattering effect. Moreover, SWCNTs undergo thermal expansion/contraction when temperature changes and the structure deteriorates. The coefficient of thermal expansion can be either positive or negative at low temperatures, but it is mostly positive at higher temperatures [30-32]. The expansion (or contraction) due to temperature change can lead to changes in the dimensions of the nanotubes, affecting the interaction and the contacts between the nanotubes. Consequently, with reduced temperature, τ_i becomes smaller, leading to an increase in Θ. As a result, the α of the SWCNT film decreases with temperature reduction. The R-T of the SWCNT film is shown to the right axis in Fig. 7a. Starting from $T =$ 290 K, the resistance of the sample gradually increases with slight ups and downs from ~831 Ω to ~1205 Ω until $T = 50$ K. At $T = 40$ K, the resistance steeply rises to ~5.01 kΩ. This abrupt change might have happened due to the structure deterioration. Also, at this point, the thermal diffusivity experiences a quick decrease with decreased temperature, confirming this structure deterioration. Afterwards, the resistance declines and fluctuates in the vicinity of ~3.08 kΩ for $12 \leq T < 40$k.

5. Conclusion

In this work, the TET technique was further developed for measuring the thermal diffusivity of semiconductive materials, e.g. GreF and SWCNT films over a broad temperature range. Intriguingly, for each sample, it was observed that a switch came about in the trend of resistance-temperature response at a specific temperature. This brought

about some abnormal shapes of TET signals compared with the pure increasing/decreasing TET signals. By establishing a physical model for the assessment of the acquired resistance-temperature (voltage-time) responses, a TET mathematical model was developed with considering the nonlinear correlation between the resistance and temperature. This model was validated using finite volume-based numerical modeling. For the GreF, the new model was used to determine the missing α that cannot be determined using the traditional TET model. The determined α perfectly follows the overall $\alpha \sim T$ trend. Over a temperature range of 84.5–690.9 K, α changed from 1.57×10^{-3} $m^2 s^{-1}$ to 1.61×10^{-4} $m^2 s^{-1}$ for the GreF. This reduction was explained by the Umklapp phonon-phonon scattering dominance at higher temperatures. For the SWCNT film, the abnormal TET signals were fitted very well using the new TET model to determine α. By measuring α using different current values, we were able to determine the α at zero temperature rise. This new strategy and methodology is critical to determining α at a specified ambient temperature, especially when R is less sensitive to T change. The α of the SWCNT film decreased from 1.81×10^{-5} to 4.0×10^{-6} $m^2 s^{-1}$ when T decreased from 290 to 12 K. This is mainly due to deteriorated film structure that is caused by thermal expansion/contraction of the SWCNTs.

CRediT authorship contribution statement

Amin Karamati: Writing – original draft, Investigation, Formal analysis, Data curation. **Meng Han:** Writing – review & editing, Validation, Supervision, Investigation, Formal analysis, Data curation, Conceptualization. **Xinyue Duan:** Writing – review & editing, Methodology, Investigation, Formal analysis, Data curation. **Yangsu Xie:** Writing – review & editing, Methodology, Investigation, Formal analysis, Data curation, Conceptualization. **Xinwei Wang:** Writing – review & editing, Writing – original draft, Validation, Supervision, Software, Resources, Project administration, Methodology, Investigation, Funding acquisition, Formal analysis, Data curation, Conceptualization.

Declaration of competing interest

The authors declare that they have no known competing financial interests or personal relationships that could have appeared to influence the work reported in this paper.

Data availability

Data will be made available on request.

Acknowledgment

Partial support of this work by the US National Science Foundation (CMMI2032464) is gratefully acknowledged.

References

[1] Y. Zheng, H. Zhao, Y. Cai, B. Jurado-Sánchez, R. Dong, Recent advances in one-dimensional micro/nanomotors: fabrication, propulsion and application, Nano-Micro Lett. 15 (1) (2023) 20.
[2] Y. Hou, Z. Gao, Y.S. Zhao, Y. Yan, Organic micro/nanoscale materials for photonic barcodes, Org. Chem. Front. 7 (18) (2020) 2776–2788.
[3] J. Guo, Y. Lin, One-dimensional micro/nanomotors for biomedicine: delivery, sensing and surgery, Biomater. Transl. 1 (1) (2020) 18.
[4] A. Elahi, S. Chaudhuri, Computational fluid dynamics modeling of the filtration of 2D materials using hollow fiber membranes, ChemEngineering 7 (6) (2023) 108.
[5] A. Karamati, S. Xu, H. Lin, M. Rahbar, X. Wang, Thermophysical properties of 1D materials: transient characterization down to atomic level, JUSTC 53 (10) (2023) 1001.
[6] H. Lin, X. Liu, A. Kou, S. Xu, H. Dong, One-dimensional thermal characterization at the micro/nanoscale: review of the TET technique, Int. J. Thermophys. 40 (2019) 1–17.
[7] J. Guo, X. Wang, T. Wang, Thermal characterization of microscale conductive and nonconductive wires using transient electrothermal technique, J. Appl. Phys. 101 (6) (2007) 063537.
[8] A. Karamati, N. Hunter, H. Lin, H. Zobeiri, S. Xu, X. Wang, Strong linearity and effect of laser heating location in transient photo/electrothermal characterization of micro/nanoscale wires, Int. J. Heat. Mass Transf. 198 (2022) 123393.
[9] A. Karamati, et al., Temperature dependence of resistivity of carbon micro/nanostructures: microscale spatial distribution with mixed metallic and semiconductive behaviors, J. Appl. Phys. 134 (8) (2023) 085102.
[10] H. Lin, N. Hunter, H. Zobeiri, Y. Yue, X. Wang, Ultra-high thermal sensitivity of graphene microfiber, Carbon 203 (2023) 620–629, https://doi.org/10.1016/j.carbon.2022.12.013.
[11] R. Wang, et al., Anisotropic thermal conductivities and structure in lignin-based microscale carbon fibers, Carbon 147 (2019) 58–69, https://doi.org/10.1016/j.carbon.2019.02.064.
[12] Y. Xie, H. Zobeiri, L. Xiang, G. Eres, J. Wang, X. Wang, Dual-pace transient heat conduction in vertically aligned carbon nanotube arrays induced by structure separation, Nano Energy 90 (2021) 106516, https://doi.org/10.1016/j.nanoen.2021.106516.
[13] S. Xu, H. Zobeiri, N. Hunter, H. Zhang, G. Eres, X. Wang, Photocurrent in carbon nanotube bundle: graded seebeck coefficient phenomenon, Nano Energy 86 (2021) 106054, https://doi.org/10.1016/j.nanoen.2021.106054.
[14] Y. Xie, et al., 19-Fold thermal conductivity increase of carbon nanotube bundles toward high-end thermal design applications, Carbon 139 (2018) 445–458.
[15] J. Gao, H. Zobeiri, H. Lin, D. Xie, Y. Yue, X. Wang, Coherency between thermal and electrical transport of partly reduced graphene paper, Carbon 178 (2021) 92–102.
[16] B. Zhu, et al., Thermal conductivity of SiC microwires: effect of temperature and structural domain size uncovered by 0 K limit phonon scattering, Ceram. Int. 44 (10) (2018) 11218–11224.
[17] C. Deng, et al., In situ investigation of annealing effect on thermophysical properties of single carbon nanocoil, Int. J. Heat. Mass Transf. 151 (2020) 119416.
[18] Q. Alahmad, M. Rahbar, M. Han, H. Lin, S. Xu, X. Wang, Thermal conductivity of gas diffusion layers of PEM fuel cells: anisotropy and effects of structures, Int. J. Thermophys. 44 (11) (2023) 167.
[19] Q. Alahmad, M. Rahbar, A. Karamati, J. Bai, X. Wang, 3D strongly anisotropic intrinsic thermal conductivity of polypropylene separator, J. Power Sources 580 (2023) 233377, https://doi.org/10.1016/j.jpowsour.2023.233377.
[20] Y. Xie, P. Yuan, T. Wang, N. Hashemi, X. Wang, Switch on the high thermal conductivity of graphene paper, Nanoscale 8 (40) (2016) 17581–17597.
[21] M. Han, et al., Strong correlation between electrical and thermal transport properties in graphene/graphite films beyond the Wiedemann–Franz law, Carbon 195 (2022) 319–327.
[22] Y. Xie, S. Xu, Z. Xu, H. Wu, C. Deng, X. Wang, Interface-mediated extremely low thermal conductivity of graphene aerogel, Carbon 98 (2016) 381–390.
[23] H. Lin, R. Wang, H. Zobeiri, T. Wang, S. Xu, X. Wang, The in-plane structure domain size of nm-thick $MoSe_2$ uncovered by low-momentum phonon scattering, Nanoscale 13 (16) (2021) 7723–7734.
[24] J. Liu, Z. Xu, Z. Cheng, S. Xu, X. Wang, Thermal conductivity of ultrahigh molecular weight polyethylene crystal: defect effect uncovered by 0 K limit phonon diffusion, ACS. Appl. Mater. Interfaces 7 (49) (2015) 27279–27288.
[25] Y. Xie, et al., The defect level and ideal thermal conductivity of graphene uncovered by residual thermal reffusivity at the 0 K limit, Nanoscale 7 (22) (2015) 10101–10110.
[26] C. Deng, et al., Thermal diffusivity of a single carbon nanocoil: uncovering the correlation with temperature and domain size, ACS Nano 10 (10) (2016) 9710–9719.
[27] B.H. Armstrong, N processes, the relaxation-time approximation, and lattice thermal conductivity, Phys. Rev. B 32 (6) (1985) 3381.
[28] J. Callaway, Model for lattice thermal conductivity at low temperatures, Phys. Rev. 113 (4) (1959) 1046.
[29] M. Rahbar, et al., Observing grain boundary-induced phonons mean free path in highly aligned SWCNT bundles by low-momentum phonon scattering, Cell Rep. Phys. Sci. 4 (12) (2023) 101688.
[30] L. Deng, et al., Coefficient of thermal expansion of carbon nanotubes measured by Raman spectroscopy, Appl. Phys. Lett. 104 (5) (2014) 051907.
[31] N. Hu, et al., Prediction of thermal expansion properties of carbon nanotubes using molecular dynamics simulations, Comput. Mater. Sci. 54 (2012) 249–254.
[32] J.-W. Jiang, J.-S. Wang, B. Li, Thermal expansion in single-walled carbon nanotubes and graphene: nonequilibrium Green's function approach, Phys. Rev. B 80 (20) (2009) 205429.